Lawrence Berkeley National Laboratory

Title

SCAT uncovers ATLAS's first tidal disruption event ATLAS18mlw: a faint and fast TDE in a quiescent Balmer strong Galaxy

Permalink

https://escholarship.org/uc/item/67p288p2

Journal

ISSN

Authors

Hinkle, Jason T
Tucker, Michael A
Shappee, Benjamin J
et al.

Publication Date

DOI

SCAT uncovers ATLAS's first tidal disruption event ATLAS18mlw: a faint and fast TDE in a quiescent Balmer strong Galaxy

Jason T. Hinkle [1]★ Michael A. Tucker [1]† Benjamin. J. Shappee [1] Thomas W.-S. Holoien [2]‡
Patrick J. Vallely [3] Thomas de Jaeger [1] Katie Auchettl [4,5,6] Greg Aldering [7] Chris Ashall [1]
Dhvanil D. Desai [1] Aaron Do [1] Anna V. Payne [1]§ and John L. Tonry [1]

[1]*Institute for Astronomy, University of Hawai'i, 2680 Woodlawn Drive, Honolulu, HI 96822, USA*
[2]*The Observatories of the Carnegie Institution for Science, 813 Santa Barbara Street, Pasadena, CA 91101, USA*
[3]*Department of Astronomy, The Ohio State University, 140 West 18th Avenue, Columbus, OH 43210, USA*
[4]*School of Physics, The University of Melbourne, Parkville, VIC 3010, Australia*
[5]*ARC Centre of Excellence for All Sky Astrophysics in 3 Dimensions (ASTRO 3D) , Sydney 2006, Australia*
[6]*Department of Astronomy and Astrophysics, University of California, Santa Cruz, CA 95064, USA*
[7]*Lawrence Berkeley Nal Laboratory, 1 Cyclotron Rd., Berkeley, CA 94720, USA*

ABSTRACT

We present the discovery that ATLAS18mlw was a tidal disruption event (TDE) in the galaxy WISEA J073544.83+663717.3, at a luminosity distance of 334 Mpc. Initially discovered by the Asteroid Terrestrial Impact Last Alert System (ATLAS) on 2018 March 17.3, the TDE nature of the transient was uncovered only recently with the re-reduction of a SuperNova Integral Field Spectrograph (SNIFS) spectrum. This spectrum, taken by the Spectral Classification of Astronomical Transients (SCAT) survey, shows a strong blue continuum and a broad H α emission line. Here, we present roughly 6 yr of optical survey photometry beginning before the TDE to constrain active galactic nucleus activity, optical spectroscopy of the transient, and a detailed study of the host galaxy properties through analysis of archival photometry and a host spectrum. ATLAS18mlw was detected in ground-based light curves for roughly 2 months. From a blackbody fit to the transient spectrum and bolometric correction of the optical light curve, we conclude that ATLAS18mlw is best explained by a low-luminosity TDE with a peak luminosity of $\log(L \, [\mathrm{erg\,s^{-1}}]) = 43.5 \pm 0.2$. The TDE classification is further supported by the quiescent Balmer strong nature of the host galaxy. We also calculated the TDE decline rate from the bolometric light curve and find $\Delta L_{40} = -0.7 \pm 0.2$ dex, making ATLAS18mlw a member of the growing class of 'faint and fast' TDEs with low peak luminosities and fast decline rates.

Key words: black hole physics – galaxies: nuclei – galaxies: supermassive black holes – transients: tidal disruption events.

1 INTRODUCTION

When a star passes within the tidal radius of a supermassive black hole (SMBH), the self-gravity of the star is overwhelmed by tidal forces and the star is disrupted, resulting in a tidal disruption event (TDE; Rees 1988; Evans & Kochanek 1989; Phinney 1989). A TDE results in a luminous flare as the disrupted stellar material falls back on to the SMBH (e.g. Ulmer 1999). To date, ∼60 of these flares have been observed (Gezari 2021), with a majority discovered in the optical. This is in large part due to the recent expansion of transient surveys such as the All-Sky Automated Survey for Supernovae (ASAS-SN; Shappee et al. 2014; Kochanek et al. 2017), the Asteroid Terrestrial Impact Last Alert System (ATLAS; Tonry et al. 2018), Gaia Alerts (Wyrzykowski et al. 2012), the Panoramic Survey

Telescope and Rapid Response System (Pan-STARRS; Chambers et al. 2016), and the Zwicky Transient Facility (ZTF; Bellm et al. 2019).

However, it is not only optical sky surveys that play an important role in discovering TDEs. Spectroscopic classification surveys are crucial in obtaining rapid spectra to not only classify transients but to also identify interesting sources. Alongside the expansion of transient surveys has been the growth of such spectroscopic surveys. In the past 2 yr, roughly three-quarters of all spectroscopically confirmed transients have been classified by the ZTF classification efforts (e.g. Fremling et al. 2020, 2021), the Public ESO Spectroscopic Survey for Transient Objects (PESSTO; Smartt et al. 2015) and successors (e.g. Barbarino et al. 2019), and the Spectral Classification of Astronomical Transients (SCAT) survey (Tucker et al. 2022), in that order.

Spectroscopic classification of TDEs has become easier as our understanding of the typical observed emission from TDEs becomes more complete. The emission of TDEs is hot, typically exhibiting a blue optical continuum, with a UV excess. The UV/optical spectral energy distribution (SED) of TDEs is often well fit by a blackbody with a temperature of the order of $T = 20\,000$–$50\,000$ K (e.g. Holoien

★ E-mail: jhinkle6@hawaii.edu
† DOE CSGF Fellow.
‡ NHFP Einstein Fellow.
§ NASA Fellowship Activity Fellow.

et al. 2014, 2016; Blagorodnova et al. 2017; Hinkle et al. 2021a). Roughly half of optically selected TDEs show X-ray emission, commonly in the form of a blackbody with kT ∼50 eV, or a soft power law with a photon index of ≳2.5 (Auchettl, Guillochon & Ramirez-Ruiz 2017; Brown et al. 2017; Auchettl, Ramirez-Ruiz & Guillochon 2018). The characteristic lifetime of a TDE in the optical bands is of the order of a few months (e.g. Hinkle et al. 2020; van Velzen et al. 2020) although UV emission can exist above host galaxy levels for several years after disruption (e.g. van Velzen et al. 2019).

TDEs represent an excellent opportunity to study otherwise non-active SMBHs. For example, TDE emission is likely sensitive to black hole spin and mass (e.g. Ulmer 1999; Graham et al. 2001; Gafton & Rosswog 2019; Mockler, Guillochon & Ramirez-Ruiz 2019). It has been shown that the SMBH masses obtained through fits to TDE light curves are consistent with those derived through other means (Mockler et al. 2019). As the large majority of SMBHs are not active (∼90 per cent; Ho 2008; Lacerda et al. 2020), this agreement suggests that TDEs may provide an important method of probing quiescent SMBHs at large distances.

Unfortunately, TDEs are rare, with observational rates estimated to be between 10^{-4} and 10^{-5} yr^{-1} per galaxy (e.g. van Velzen & Farrar 2014; Holoien et al. 2016; Auchettl et al. 2018; van Velzen 2018). Interestingly, TDEs seem to prefer particular host galaxies where a recent burst of star formation has occurred (e.g. French, Arcavi & Zabludoff 2016; Stone & van Velzen 2016) and moderately massive stars may be preferred (Mockler et al. 2022). These include quiescent Balmer strong (QBS) and post-starburst (PSB) galaxies, both likely post-merger systems (French 2021). TDEs occur at rates enhanced by factors of roughly 20 and 40 times the typical values for QBS and PSB galaxies, respectively (e.g. Arcavi et al. 2014; French et al. 2016, 2020b; Law-Smith et al. 2017; Graur et al. 2018). Furthermore, Arcavi, Nyiha & French (2022) find that the relative contamination of Type Ia SNe to TDEs is decreased by a factor of ∼2.7 in QBS or PSB galaxies as compared to quiescent galaxies.

Due in part to the preference for TDEs to occur in unique galaxies and their slightly increased rates around lower mass SMBHs (Wang & Merritt 2004; Stone & Metzger 2016; van Velzen 2018), the host galaxies of TDEs have received special attention (Law-Smith et al. 2017; French et al. 2020a, b). To fulfil the promise of TDEs as probes of SMBHs, studies of the history of accretion, mergers, and star-formation in the TDE host galaxies are needed (e.g. Prieto et al. 2016).

Here, we present the observations of the first TDE discovered by ATLAS, ATLAS18mlw. The paper is organized in the following manner. In Section 2, we detail observations of the TDE candidate and host galaxy. In Section 3, we discuss the properties of the host galaxy of ATLAS18mlw. In Section 4, we analyse the data on this source, and in Section 5 we discuss our results. Throughout this paper, we have used a cosmology with $H_0 = 69.6$ km s^{-1} Mpc^{-1}, $\Omega_M = 0.29$, and $\Omega_\Lambda = 0.71$ (Wright 2006; Bennett et al. 2014).

2 DATA

2.1 Archival photometry

We obtained archival photometry of the host galaxy WISEA J073544.83+663717.3 including *ugriz* magnitudes from the Sloan Digital Sky Survey (SDSS) Data Release 15 (Aguado et al. 2019) and *W*1 and *W*2 magnitudes from the Wide-field Infrared Survey Explorer (WISE; Wright et al. 2010) AllWISE catalogue. While the host galaxy was not listed in any Galaxy Evolution Explorer (GALEX; Martin et al. 2005) catalogue, we measured a 6.0 arcsec

Table 1. Archival host-galaxy photometry.

Filter	Magnitude	Magnitude uncertainty
FUV	>23.56	3σ
NUV	23.66	0.34
u	21.76	0.23
g	20.08	0.03
r	19.34	0.02
i	18.96	0.02
z	18.79	0.06
*W*1	19.04	0.06
*W*2	19.46	0.16

Note. Archival magnitudes of the host galaxy WISEA J073544.83+663717.3. The *FUV* and *NUV* magnitudes were measured from GALEX images, the *ugriz* magnitudes are taken from the SDSS catalogue and the *W*1 and *W*2 magnitudes are taken from the AllWISE catalogue. All magnitudes are presented in the AB system.

radius aperture *FUV* and *NUV* limit and magnitude from GALEX images using gPhoton (Million et al. 2016). These ultraviolet, optical, and infrared host-galaxy magnitudes and estimated uncertainties are presented in Table 1.

2.2 Transient imaging

The transient ATLAS18mlw, $(\alpha, \delta) = (07\!:\!35\!:\!44.777, +66\!:\!37\!:\!16.43)$, was discovered on 2018 March 17.3 by the ATLAS survey. The discovery was announced publicly on the Transient Name Server (TNS) and given the name AT2018ahl[1] (Tonry et al. 2018). To give appropriate credit to the discovering survey, we will refer to the transient by its survey name ATLAS18mlw throughout the remainder of this manuscript.

Soon after the ATLAS discovery, we obtained a *V*-band acquisition image with the Supernova Integral Field Spectrograph (SNIFS; Lantz et al. 2004) on the University of Hawai'i 88-in telescope (UH88). From this, we are able to compare the location of the transient to the location of the host galaxy to determine if the source is spatially consistent with the nucleus. We first used astrometry.net (Barron et al. 2008; Lang et al. 2010) to compute astrometry for both the SNIFS acquistion image and a Pan-STARRS *r*-band image (Chambers et al. 2016). We then measured the centroid of the host galaxy from the Pan-STARRS image and the centroid of the TDE in the SNIFS image with the IRAF task imcentroid. We find a transient position of $(\alpha, \delta) = (07\!:\!35\!:\!44.793, +66\!:\!37\!:\!16.53)$ and a host galaxy position of $(\alpha, \delta) = (07\!:\!35\!:\!44.769, +66\!:\!37\!:\!16.34)$. Combined, these give an offset of 0.4 arcsec ± 0.5 arcsec, where the uncertainty is dominated by the uncertainties in the astrometric solutions for the SNIFS and Pan-STARRS images. At the host distance, this offset corresponds to a physical distance of 600 ± 700 pc, consistent with ATLAS18mlw being a nuclear transient.

We then obtained the ATLAS light curves of ATLAS18mlw from the ATLAS forced point spread function (PSF) photometry service. ATLAS uses two 0.5-m telescopes located on Haleakalā and at the Mauna Loa Observatory. During typical operation, the ATLAS telescopes obtain four 30 s exposures covering roughly a quarter of the sky per night (Smith et al. 2020). ATLAS obtains images in two broad-band filters, the 'cyan' (*c*) filter from 420–650 nm and the

[1] https://www.wis-tns.org/object/2018ahl
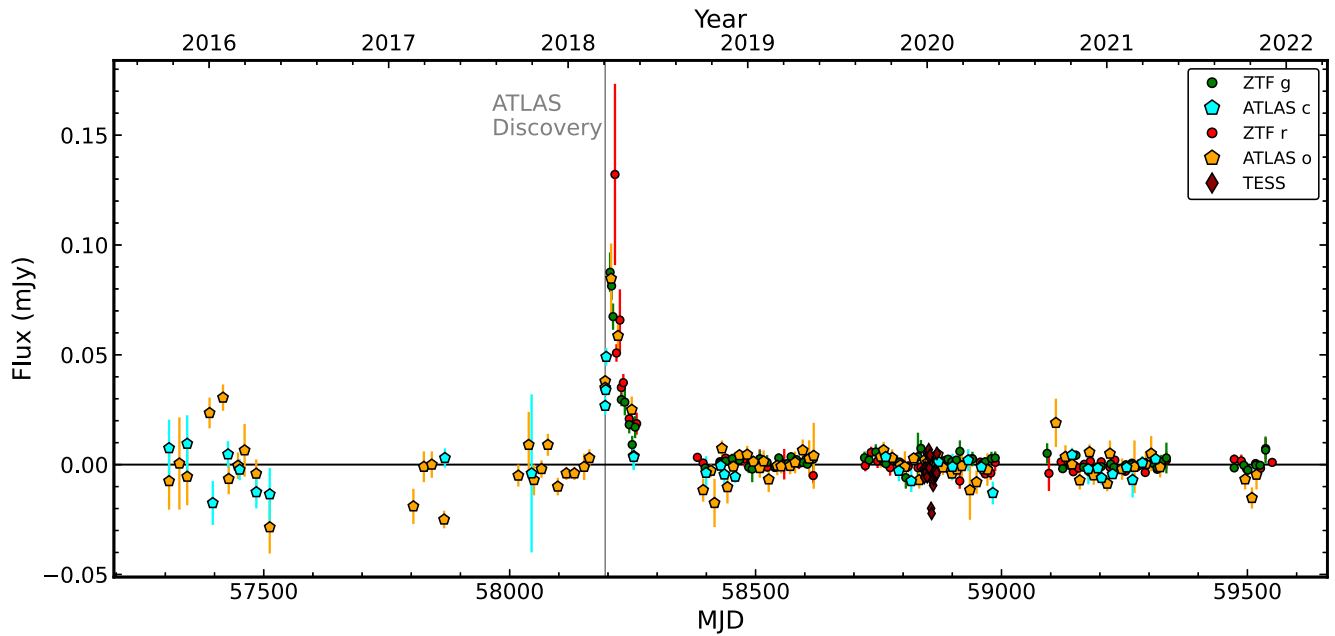
Figure 1. Host-subtracted and Galactic-extinction-corrected light curve of the host galaxy WISEA J073544.83+663717.3 from ATLAS, ZTF, and TESS spanning approximately 6 yr. The ATLAS18mlw flare is clearly visible during early 2018. The green and red circles represent ZTF *g*- and *r*-band photometry stacked in 1-d bins during the flare and 10-d bins outside of the flare. The cyan and orange circles represent ATLAS *c*- and *o*-band photometry stacked in 1-d bins during the flare and 10-d bins outside of the flare. The dark red circles represent TESS photometry stacked in 1-d bins. The vertical grey line marks the epoch of ATLAS discovery.

'orange' (*o*) filter from 560–820 nm (Tonry et al. 2018). We combine intra-night epochs using a weighted mean to obtain deeper limits and more robust detections.

In addition to ATLAS photometry, we obtained ZTF photometry in the *g* and *r* bands from their forced PSF photometry service. The ZTF survey uses the Samuel Oschin 48-in telescope at the Palomar Observatory. In normal operation, ZTF images down to a depth of ∼20.5 *r*-band mag in a 30 s exposure (Bellm et al. 2019). Similar to the ATLAS data, we combined the intra-night photometric observations using a weighted average to get a single flux measurement.

We also obtained a light curve of the host galaxy from the Transiting Exoplanet Survey Satellite (TESS; Ricker et al. 2015). TESS observed the location of ATLAS18mlw during Sector 20, at a phase of approximately 650 d after discovery. The TESS full frame images (FFIs) were reduced using the ISIS package (Alard & Lupton 1998; Alard 2000). We performed image subtraction following the procedures of Vallely et al. (2019, 2021) to compute our differential light curves. The reference image was constructed from the first 100 FFIs of good quality. The measured count rates were converted into fluxes using the instrumental zero-point of 20.44 electrons per second (Vanderspek et al. 2018). To quantify the host variability, we binned the TESS data in 12 h bins and computed the root mean squared (RMS) scatter, finding a value of 8.1 μJy. From this RMS scatter and assuming a variability fraction of 5 per cent, we find a limit on a possible active galactic nucleus (AGN) luminosity in the TESS band of $\lesssim 9 \times 10^{43}$ erg s^{-1}.

Finally, we obtained ASAS-SN photometry in the *g* and *V* bands from the newly public subtracted light-curve server[2] (Kochanek et al. 2017). Over the full baseline of the ASAS-SN survey, the host galaxy of ATLAS18mlw was imaged 285 times in *V* and 349 times in *g* with

no images showing significant detections. The median 5σ upper limits are 17.6 and 18.0 mag for the *V* and *g* bands, respectively.

Fig. 1 shows the ATLAS, ZTF, and TESS data for ATLAS18mlw both during the flare and in periods of quiescence. Here, the ATLAS and ZTF data have been stacked in 1-d bins during the flare and 10-d bins outside of the flare, and the TESS data have been stacked in 1 d bins. Besides the ATLAS18mlw flare itself, it is apparent that no other large flare exists in the roughly 6 yr of coverage. This suggests that the host galaxy did not exhibit AGN-like activity prior to the detection of ATLAS18mlw.

The subset of the light curve during the ATLAS18mlw flare is shown in Fig. 2, showing that ATLAS18mlw rose to peak within ∼10 d after discovery, although there are no non-detections near the discovery epoch to help constrain the time of first light further. After peak, the transient fades by 2 mag within 60 d and is not detected afterwards. This is faster than most TDEs, although there is no simultaneous UV coverage to test the longevity of the UV excess commonly seen in TDEs (e.g. Holoien et al. 2016; van Velzen et al. 2020; Gezari 2021).

2.3 Spectroscopy

A classification spectrum was obtained 1.05 d after discovery by the SCAT survey (Tucker et al. 2018, 2022) using SNIFS on UH88. SNIFS is comprised of a blue (B; 320–560 nm) and red (R; 520–1000 nm) channel. The original classification spectrum was reduced with a summit-based quick-look pipeline which is a simplified version of the full SNfactory pipeline (Aldering et al. 2006). The quick-look pipeline estimates the extraction location by averaging over the wavelength axis in each channel and then does aperture photometry.

The quick-look pipeline is reliable when the wavelength dependence of the trace position is less than the seeing. This is true for

[2]https://asas-sn.osu.edu/
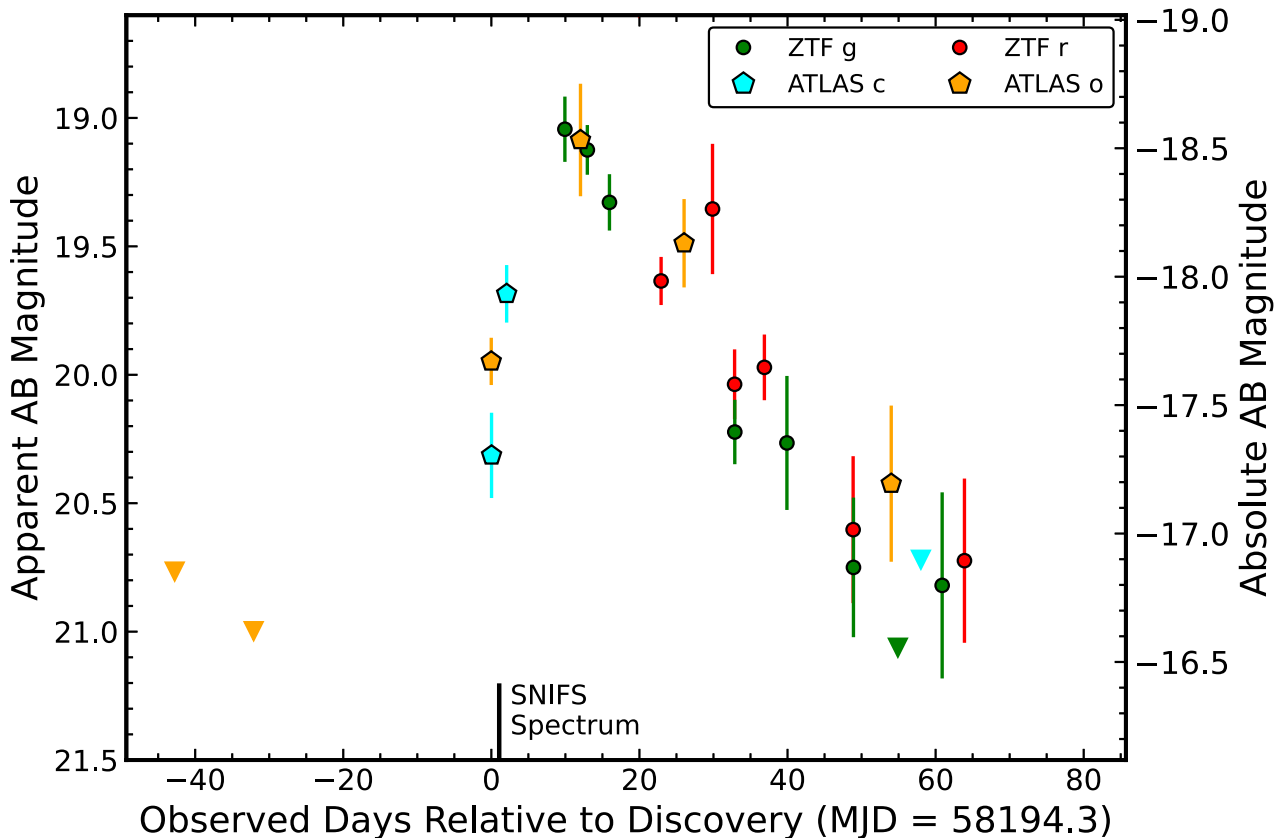
Figure 2. Host-subtracted and Galactic-extinction-corrected optical light curves of ATLAS18mlw. Shown are ATLAS (*co*) and ZTF (*gr*) photometry stacked in 1-d bins. The downward-facing triangles indicate 3σ upper limits in filters of the same respective colour. The thick black bar on the bottom axis marks the epoch of the initial SNIFS spectrum. All data are shown in the AB magnitude system.

targets observed near zenith, but atmospheric dispersion shifts the object's location on the chip as the airmass increases. ATLAS18mlw was observed at an airmass of $\approx$1.62 which introduced a wavelength-dependence to the relative contributions from the TDE and the host-galaxy to the final spectrum, masking the transient's signal and hindering classification.

The development of an upgraded reduction pipeline at the University of Hawai'i in 2021 June incorporates wavelength-dependent tracing across each channel. Reanalysis of the classification spectrum revealed a strong blue continuum with narrow host lines and a broad Hα line at a redshift of $z = 0.073$. A full description of the updated reduction pipeline is presented in Tucker et al. (2022). At this redshift, the peak absolute magnitude is -18.6 mag. We see none of the broad absorption lines commonly seen in various classes of Type I supernovae (Filippenko 1997). Additionally, the luminous peak absolute magnitude and lack of a plateau phase in the redder bands likely rule out Type II supernovae (e.g. Galbany et al. 2016). Combined, the spectral features and peak absolute magnitude of ATLAS18mlw are consistent with a TDE (e.g. van Velzen et al. 2020; Gezari 2021).

After concluding that ATLAS18mlw was likely a TDE, we obtained a spectrum of the host galaxy WISEA J073544.83+663717.3 with the Gemini Multi-Object Spectrograph (GMOS; Hook et al. 2004) on the 8.1-m Gemini North telescope. This spectrum was taken with the B600 grating and dithered both along the spatial and spectral directions to mitigate the presence of chip gaps and avoid the influence of bad pixels. The spectra were reduced using normal methods such as bias, flat-fielding, and wavelength calibration using

arc lamps. The individual dithered spectra were median combined to minimize the effect of cosmic ray hits. Fig. 3 shows the SNIFS and GMOS spectra with common TDE and AGN emission lines marked.

With this deeper and higher resolution GMOS spectrum we fit for the redshift the methods of Hayden et al. (2021). This method consists of a weighted cross-correlation (Kelson et al. 2000) between our observed spectrum and galaxy templates from SDSS.[3] Using the weighted average of six binning choices from 5 to 20 Å we find an average observed redshift of $z = 0.0734 \pm 0.0004$, which we will adopt for the remainder of our analysis. Stellar absorption lines such as the G band (4304 Å), Mg I (5175 Å), and Na I (5890 Å) were used to determine the redshift. This redshift implies a luminosity distance of 334 Mpc and an angular scale of $\sim$1.41 kpc arcsec^{-1}.

3 HOST-GALAXY PROPERTIES

To better understand the host galaxy, we fit stellar population synthesis models to the archival photometry of WISEA J073544.83+663717.3 (shown in Table 1), excluding the *FUV* limit. We used the Fitting and Assessment of Synthetic Templates (FAST; Kriek et al. 2009) code to obtain an SED for the host galaxy. In this fit we assumed a Cardelli, Clayton & Mathis (1989) extinction law with $R_V = 3.1$ and a foreground Galactic extinction of $A_V = 0.113$ mag (Schlafly & Finkbeiner 2011), a Salpeter initial mass function (Salpeter 1955), an exponentially declining star formation rate, and

[3] http://classic.sdss.org/dr5/algorithms/spectemplates/
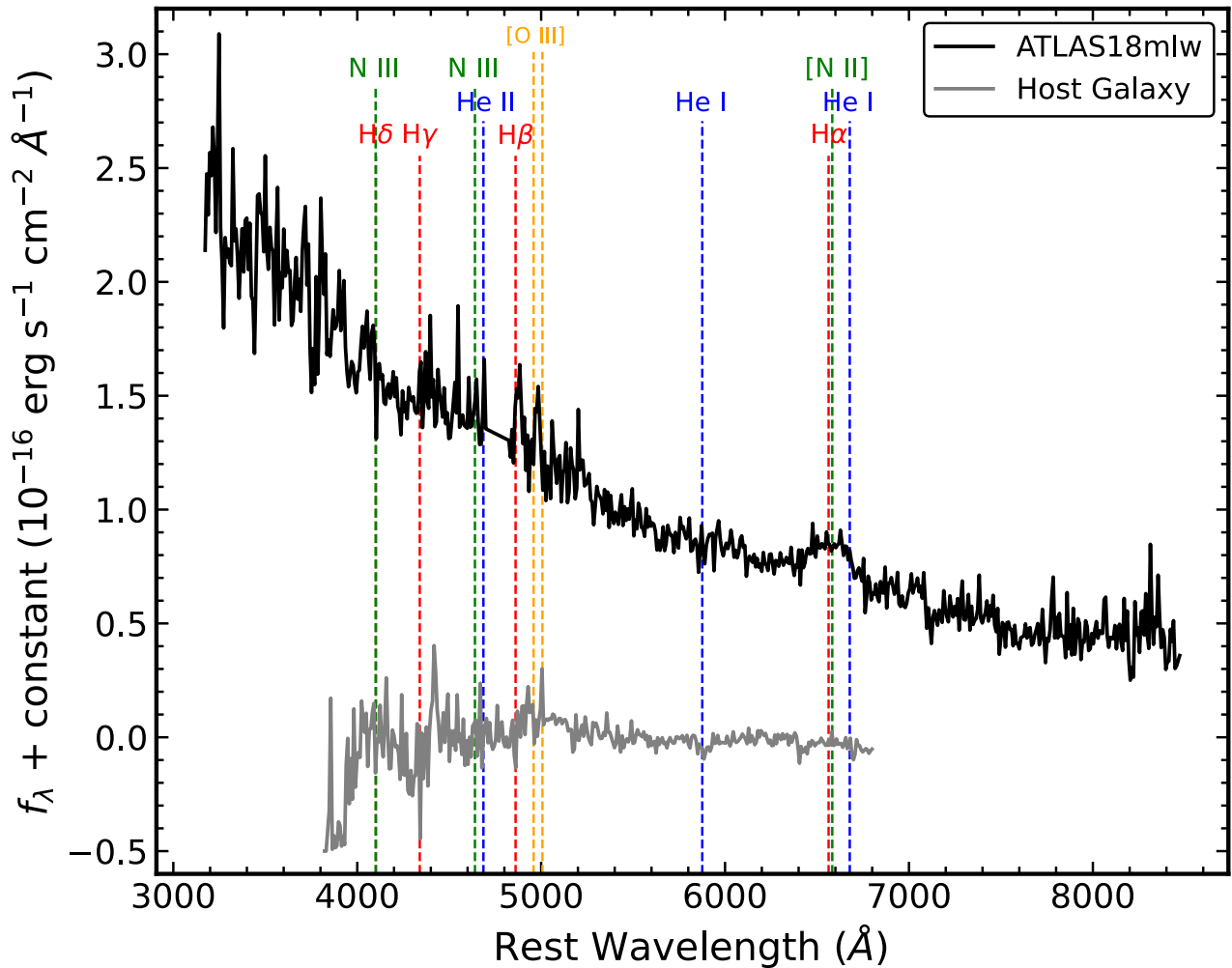
Figure 3. Optical spectra of ATLAS18mlw (black line) and the host galaxy WISEA J073544.83+663717.3 (grey line). The vertical lines mark spectral features common in TDEs and AGNs, with hydrogen lines in red, helium lines (He II λ 4686, He I λ 5876, and He I λ 6678) in blue, nitrogen lines (N III λ 4100, N III λ 4640, and [N II] λ 6583) in green, and oxygen lines [(O III) λ 4959 and (O III) λ 5007] in orange. Both spectra have been binned in ∼9 Å bins and the dichroic crossover region has been masked out for the SNIFS spectrum.

the Bruzual & Charlot (2003) stellar population models. From our FAST fit, we find that WISEA J073544.83+663717.3 has a stellar mass of $M_* = 2.8^{+0.6}_{-0.4} \times 10^9$ M$_\odot$, an age of $2.8^{+0.7}_{-0.6}$ Gyr, and a star formation rate of SFR $= 1.5^{+1.3}_{-1.1} \times 10^{-2}$ M$_\odot$ yr^{-1}.

From the commonly used scaling relationship between stellar mass and SMBH mass (McConnell & Ma 2013; Mendel et al. 2014), we estimate a central black hole mass of $\sim 10^{6.4}$ M$_\odot$, where these scaling relations have a typical scatter of ~ 0.4 dex. If we instead use the scaling of Reines & Volonteri (2015), we find a central black hole mass of $\sim 10^{5.8}$ M$_\odot$. As the scaling of Reines & Volonteri (2015) includes more low-mass galaxies, we adopt this SMBH mass throughout the remainder of the manuscript. This mass estimate is close to the median BH mass on which TDEs occur ($\sim 10^6 M_\odot$; Wevers et al. 2017; Ryu, Krolik & Piran 2020) and is also consistent with the range of SMBH masses for which TDEs occur most efficiently ($\leq 10^7 M_\odot$; van Velzen 2018).

The GMOS spectrum provides additional insight into the host-galaxy properties. We used the Penalized Pixel-Fitting code (PPXF; Cappellari & Emsellem 2004; Cappellari 2017) to simultaneously fit a stellar and gas component to the host galaxy spectrum, which

allows for robust measurements of emission line fluxes. We measured the luminosity of the narrow H α line in the GMOS spectrum and applied the scaling between SFR and H α luminosity from Osterbrock & Ferland (2006) to obtain an SFR of 3.5×10^{-3} M$_\odot$ yr^{-1}, which is smaller than, but consistent with, the value obtained from the SED fits. In addition to the bulk host galaxy properties, we can constrain the presence of AGN activity from the spectrum. From PPXF we measure an [O III] 5007λ emission line luminosity of 3.9×10^{39} erg s^{-1}. This is well below the median AGN [O III] line luminosity indicating that the host galaxy does not harbour a strong AGN, but not ruling out the presence of low-luminosity AGN (e.g. Zakamska et al. 2003; Bongiorno et al. 2010). If the host galaxy harbours an AGN, we can use the bolometric luminosity scaling of Pennell, Runnoe & Brotherton (2017) to estimate a bolometric luminosity of $\sim 3 \times 10^{44}$ erg s^{-1}, similarly lying well below the median observed value (Woo & Urry 2002; Lusso et al. 2012).

In addition to straightforward line-luminosity measurements, we use well-accepted emission-line diagnostic diagrams to understand the host galaxy properties and activity levels. Again using PPXF, we
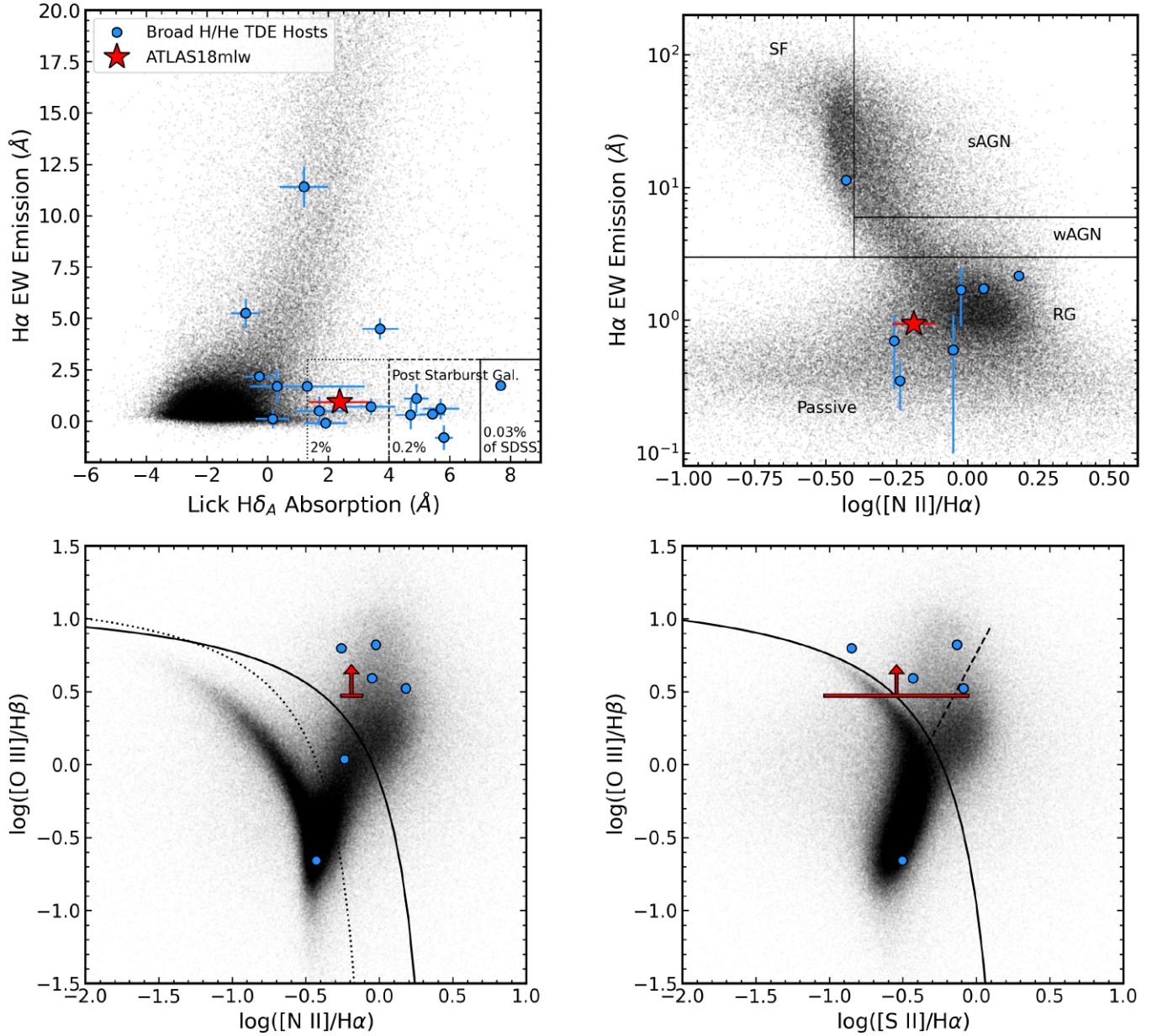
Figure 4. Line measurements of the host galaxy WISEA J073544.83+663717.3 computed from the GMOS spectrum. *Upper left panel*: Hα emission EW, tracing ongoing star formation, as compared to the Lick Hδ_A absorption index, tracing star formation over the past Gyr. The host WISEA J073544.83+663717.3 is represented by a red star and other TDE hosts are shown with blue circles. WISEA J073544.83+663717.3 is a QBS galaxy, similar to many TDE hosts. *Upper right panel*: Hα emission EW (W$_{H\alpha}$), as compared to $\log_{10}([N\,II]/H\alpha)$, otherwise known as the WHAN diagram (Cid Fernandes et al. 2011). Several lines separating star-forming galaxies (SF), strong AGN (sAGN), weak AGN (wAGN), and passive and 'retired galaxies' (RG) are shown (Cid Fernandes et al. 2011). *Lower Left Panel*: $\log_{10}([O\,III]/H\beta)$ versus $\log_{10}([N\,II]/H\alpha)$ diagram (Baldwin, Phillips & Terlevich 1981; Veilleux & Osterbrock 1987). The solid line theoretically separates AGNs (above) and H II regions (below) (Kewley et al. 2001). The dotted line empirically separates the same classifications Kauffmann et al. (2003). *Lower right panel*: $\log_{10}([O\,III]/H\beta)$ versus $\log_{10}([S\,II]/H\alpha)$ diagram (Veilleux & Osterbrock 1987). The solid line represents the same separation as before (Kewley et al. 2001). The diagonal dashed line separates Seyferts (above) and LINERs (below) (Kewley et al. 2006). WISEA J073544.83+663717.3 has only upper limits on the Hβ emission. Galaxies from the SDSS Data Release 8 (Eisenstein et al. 2011) are shown in black to illustrate the broader distribution of galaxy properties in these parameter spaces.

estimated emission line fluxes and uncertainties from the GMOS spectrum. In the upper left panel of Fig. 4 we show the Hα emission equivalent width (EW) as compared to the Lick Hδ_A absorption index. The Hα EW traces current star formation, whereas the Lick Hδ_A index traces star formation within the past Gyr. This diagram is commonly used to select post-merger and PSB systems based on their low current star formation rate but high recent star formation (e.g. French et al. 2018). The host galaxy of ATLAS18mlw has Lick

H$\delta_A \simeq 2.4 \pm 1.0$ Å, as measured by PyPHOT[4], consistent with a QBS galaxy, similar to many other TDE host galaxies.

In the upper right panel of Fig. 4 we show the Hα emission EW (W$_{H\alpha}$), as compared to $\log_{10}([N\,II]/H\alpha)$, also known as the WHAN diagram (Cid Fernandes et al. 2011). This diagram separates actively

[4]https://mfouesneau.github.io/docs/pyphot/#

star-forming and active galaxies from passive galaxies using the Hα emission EW. The galaxies with high $W_{H\alpha}$ are further separated by $\log_{10}([N\,II]/H\alpha)$ into pure star-forming galaxies and active galaxies. The host galaxy of ATLAS18mlw resides in between the retired and passive galaxies regimes, suggesting that the host does not harbour a strong AGN. Again, the host galaxy is similar in terms of its location in the WHAN diagram to other TDE hosts.

In the bottom two panels of Fig. 4 we show the traditional $\log_{10}([N\,II]\,\lambda6583/H\alpha)$ and $\log_{10}([S\,II]\,\lambda\lambda\,6717, 6731/H\alpha)$ emission-line ratio diagrams (Baldwin et al. 1981; Veilleux & Osterbrock 1987). Hβ emission was not detected in the host galaxy spectrum, and we therefore use 3σ upper limits. In both diagrams, the lower limit on $\log_{10}([O\,III]\,\lambda5007/H\beta)$ lies in the AGN/Seyfert region, but similar to other TDE hosts (Graur et al. 2018). Addition, the large uncertainty on [S II] flux leads to ambiguity on the classification of the source between a star-forming galaxy, a Seyfert, and a LINER (low-ionization nuclear emission-line region; Heckman 1980). Finally, if we assume a typical Balmer decrement of 2.86 (Osterbrock 1989) to estimate the Hβ flux from the observed Hα flux, we obtain a line ratio of $\log_{10}([O\,III]/H\beta) \simeq 0.9$.

We can also constrain the possibility of the host galaxy harbouring a strong or obscured AGN through mid-infrared colours. Using the WISE photometry of the host galaxy, we find a $W1 - W2$ colour of 0.22 ± 0.17 Vega mag. This is bluer than the 0.8 mag cut commonly imposed for AGNs (Assef et al. 2013) and consistent with the host galaxies of many TDEs and ambiguous nuclear transients (ANTs; Hinkle et al. 2021a). While the WISE data cannot rule out an AGN on its own, it is unlikely that the galaxy hosts a strong or highly obscured AGN.

Finally, we measured an X-ray flux at the position of the host galaxy using archival ROSAT (ROentgen SATellite; Voges et al. 1999) images. We find a 3σ upper limit of <0.03 counts s^{-1} in the 0.3–2.0 keV bandpass. Assuming an AGN-like photon index of 1.75 (Ricci et al. 2017) and the Galactic column density along the line of sight of 3.63×10^{20} cm^{-2} (HI4PI Collaboration 2016), we find a 0.3–10 keV limit of $<1.0 \times 10^{-12}$ erg s^{-1} cm^{-2}, which corresponds to a luminosity of $<1.3 \times 10^{43}$ erg s^{-1}. This is fully consistent with a normal AGN, and cannot solely rule out the presence of a strong AGN. Unfortunately, besides ROSAT, there is little X-ray coverage of this host galaxy to further constrain the prescence of an AGN. Nevertheless, combining emission line diagnostics, MIR colours, and the X-ray upper limit suggest that WISEA J073544.83+663717.3 is unlikely to host a strong AGN.

4 ANALYSIS

While there is relatively little data during the transient event, we can none the less place constraints on the transient evolution and understand it in the context of other TDEs. Fitting the Hα emission as a single Gaussian, we find a flux of $(7.3 \pm 1.1) \times 10^{-15}$ erg cm^{-2} s^{-1} corresponding to a line luminosity of $(9.6 \pm 1.4) \times 10^{40}$ erg s^{-1}. The EW of the line relative to the nearby continuum is 112 ± 17 Å. The width of the spectral line is $(1.5 \pm 0.3) \times 10^{4}$ km s^{-1}, all similar to known TDEs (e.g. van Velzen et al. 2020; Gezari 2021). Finally, because of the location of the SNIFS dichroic crossover region at the redshift of ATLAS18mlw, it is not possibly to cleanly detect and measure the properties of the tentative Hβ emission line.

A common analysis of optically selected TDEs is blackbody fits to their UV/optical SEDs to obtain effective temperatures and bolometric luminosities. Unfortunately, we do not have any UV photometry during the flare to probe the high-energy emission from this event directly. It is known that TDEs without UV photometry near

their peaks can have sizable uncertainties on their SED properties (e.g. Hinkle et al. 2020).

We can still make a rough estimate of these properties by fitting the optical spectrum as a blackbody. To do this, we first corrected the SNIFS spectrum for Galactic extinction. While host galaxy extinction is also important, it is difficult to estimate. Nevertheless, the WISE colours and lack of an observed Na I D absorption line in both the SNIFS and GMOS spectra indicate that nuclear dust extinction is small (e.g. Poznanski, Prochaska & Bloom 2012). The GMOS host-galaxy spectrum does not cover a wide enough range in wavelength to host-subtract the SNIFS transient spectrum. We thus fit the spectrum below $\sim$4900 Å where the host galaxy is faint and a large majority of the flux is from the transient. Additionally, fitting below 4900 Å allowed us to avoid the affects of the crossover region, where the SNIFS flux calibration is often poor and artefacts can be present.

We fit the TDE spectrum with a Markov Chain Monte Carlo (MCMC) approach with flat temperature priors of 1000 K $< T <$ 55 000 K. We assumed a blackbody model for our fit and obtained the bolometric luminosity, radius, and effective temperature. The χ^2 per degree of freedom for this fit is 1.0, indicating a good fit to the blue portion of the spectrum. The spectrum and corresponding blackbody fit are shown in Fig. 5. The fitted luminosity of $L = (1.7 \pm 0.1) \times 10^{43}$ erg s^{-1}, radius of $R = (1.1 \pm 0.1) \times 10^{15}$ cm, and temperature of $T = (1.2 \pm 0.1) \times 10^{4}$ K are also shown on the figure. These uncertainties are very likely underestimated as they only represent the statistical uncertainty on the fact and ignore the systematic affects associated with fitting only optical data for hot sources. As expected from the lack of host subtraction, the spectrum deviates from the blackbody fit at redder wavelengths.

Using the blackbody parameters computed above, we can better understand the light curve of ATLAS18mlw in the context of other TDEs. Similar to previous TDEs (Hinkle et al. 2020, 2021a; Holoien et al. 2020), we bolometrically corrected the optical light curves shown in Fig. 2 using the fitted luminosity at the time of the SNIFS spectrum. This was done by scaling the ATLAS c and ZTF g light curves to match the bolometric luminosity estimated from the SNIFS spectrum. As there was a single bolometric luminosity estimate, the scaling between the cg data and the bolometric luminosity was assumed to be constant throughout the TDE evolution. This assumes a relatively flat temperature evolution, which is often acceptable for a TDE (Gezari 2021; Hinkle et al. 2021b; van Velzen et al. 2021).

Following the procedure outlined in Hinkle et al. (2020), we computed the peak luminosity and decline rate measured at 40 d (ΔL_{40}) for ATLAS18mlw. Given the small number of epochs near peak light, we used a Monte Carlo approach to estimate the peak luminosity, fitting the data near peak 5000 times, each time with the luminosities perturbed by their uncertainties assuming Gaussian errors. This yielded a peak luminosity of $\log(L\,[\text{erg s}^{-1}]) = 43.5 \pm 0.2$. To ensure a robust uncertainty estimate given the lack of UV data, this error represents the 90 per cent confidence interval of the luminosities computed from our Monte Carlo estimation. Estimating a time of peak light with the same procedure yields $\text{MJD}_{\text{peak}} = 58204.4 \pm 6.8$, consistent with the approximate optical peak seen in Fig. 2. Given the SMBH mass estimated from the host galaxy SED fitting, this represents an Eddington ratio of $\sim$20 per cent, similar to other TDEs (e.g. Wevers et al. 2017; Mockler et al. 2019). We next computed the decline rate and found $\Delta L_{40} = -0.7 \pm 0.2$. The peak luminosity and decline rate of ATLAS18mlw, along with well-studied TDEs and ANTs, are shown in Fig. 6, with ATLAS18mlw broadly following the trend seen for TDEs (e.g. Hinkle et al. 2020, 2021a).
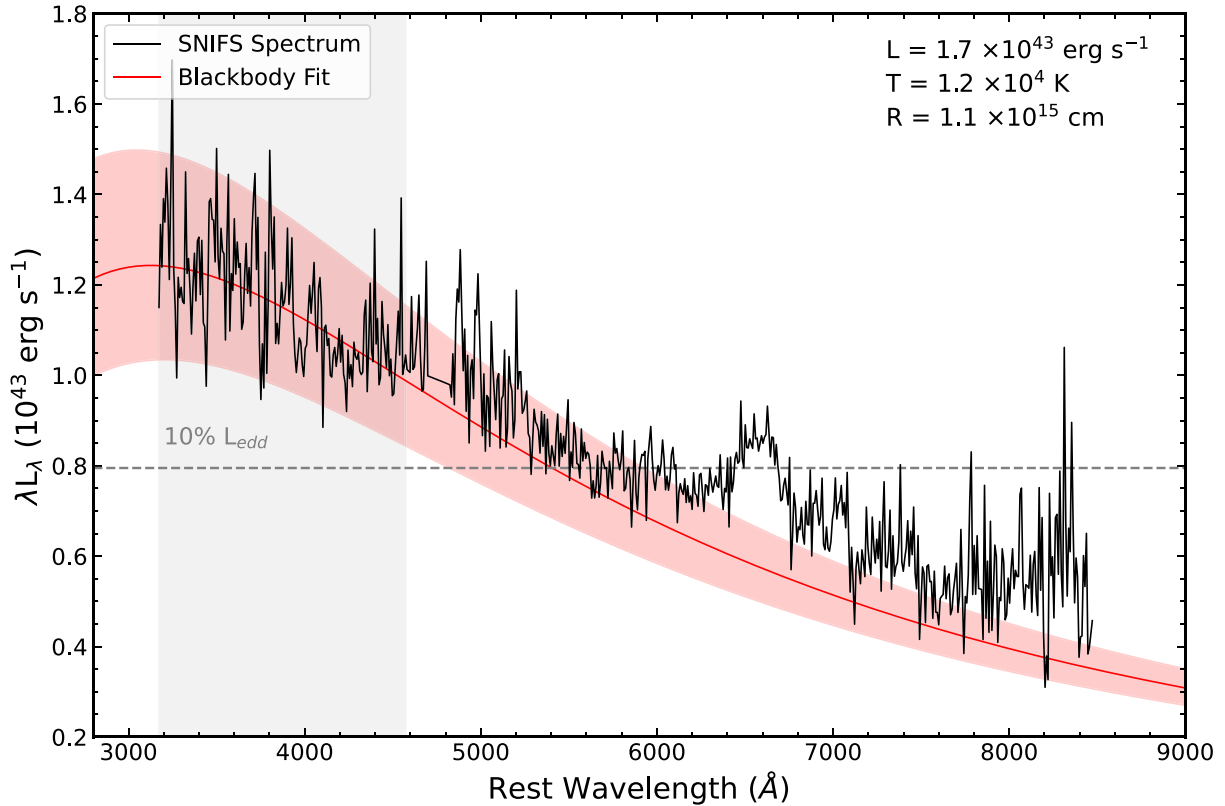
Figure 5. MCMC blackbody fit to the SNIFS spectrum of ATLAS18mlw. We present the spectrum in λL_λ to show that the TDE is clearly dominated by continuum emission in the blue and UV wavelengths. The best-fitting luminosity, temperature, and radius are shown in the upper right corner. The grey shaded area represents the portion of the spectrum that has been fit as a blackbody. The grey dashed line represents 10 per cent of the Eddington luminosity for a $10^{5.8}$ $M_\odot$ SMBH. As before, the spectrum has been binned in ~ 9 Å bins and the dichroic crossover region has been masked out.

5 DISCUSSION

The observational data of ATLAS18mlw appear similar to many other TDEs, with no significant archival host variability, a likely post-merger host galaxy, a strong blue continuum with broad emission lines near peak, and a time-scale of a few months in the optical. While we do not have direct measurements of the UV flux, the presence of strong Hα emission indicates that there must be significant far UV flux in the neighbourhood of the transient, typical of TDEs (e.g. Roth & Kasen 2018) and Seyfert galaxies (e.g. Antonucci 1993). Transients associated with AGN accretion rate changes also commonly exhibit broad Hα emission (e.g. Gezari et al. 2017; Frederick et al. 2020; Neustadt et al. 2020). As such, we must consider the possibility that ATLAS18mlw is a smooth AGN flare. First, the short overall time-scale of ATLAS18mlw is less than the roughly year-long time-scales of AGN-related flares (Hinkle et al. 2021a). Additionally, the spectrum of ATLAS18mlw is well fit as blackbody, consistent with TDEs (e.g. Holoien et al. 2014, 2016), whereas most AGNs are better fit by power laws (e.g. Vanden Berk et al. 2001; Neustadt et al. 2020). Finally, the lack of significant optical variability, weak narrow Hα emission from the host galaxy, and the relatively blue WISE colours are inconsistent with the presence of an AGN.

ATLAS18mlw also shares some characteristics with supernovae that can occur in the nuclei of their host galaxies. Most similar to ATLAS18mlw in terms of absolute magnitude are Type Ia supernovae (e.g. Folatelli et al. 2010). However, the optical spectrum of ATLAS18mlw does not have any of the expected absorption lines seen for any class of Type I supernova (Filippenko 1997). Conversely,

Type II supernovae do show an early blue continuum and broad Hα emission. However, the photometric evolution of ATLAS18mlw is unlike typical Type II supernova, being both more luminous and faster evolving than the large majority of Type II supernovae (e.g. Galbany et al. 2016). Additionally, we note that the light curves of supernovae occurring in an AGN disc may be similar to the light curve of ATLAS18mlw in terms of time-scale and luminosity (Grishin et al. 2021). However, theoretical predictions on the spectra of these transients are needed to disentangle such a scenario from the TDE scenario favoured here due to the agreement between the properties of ATLAS18mlw and its host galaxy with known TDEs.

With ATLAS18mlw as a TDE candidate rather than an AGN flare or supernova, we can compare its properties to well-observed TDEs in the literature. Using the optical spectroscopic classification scheme of Leloudas et al. (2019) and van Velzen et al. (2021), this TDE would likely be a TDE-H due to the dominance of Hα over any other spectral feature. TDE-H objects tend to have broader lines than TDE-Bowen objects (Charalampopoulos et al. 2022a), consistent with the Hα line width computed for ATLAS18mlw. The $\sim 15\,000$ km s^{-1} Hα line seen for ATLAS18mlw lies at the median value seen for TDE-H objects, and a factor of a few higher than the median Hα line width for TDE-Bowen objects (Charalampopoulos et al. 2022a). However, some TDEs, like ASASSN-15oi (Holoien et al. 2018) and ASASSN-19dj (Hinkle et al. 2021b), show signs for changes in spectral features and the properties of observed emission lines, which we cannot probe for ATLAS18mlw with our single spectrum. Nevertheless, the appearance of the broad Hα line at an approximate phase of 9 d before peak for ATLAS18mlw is among the earliest
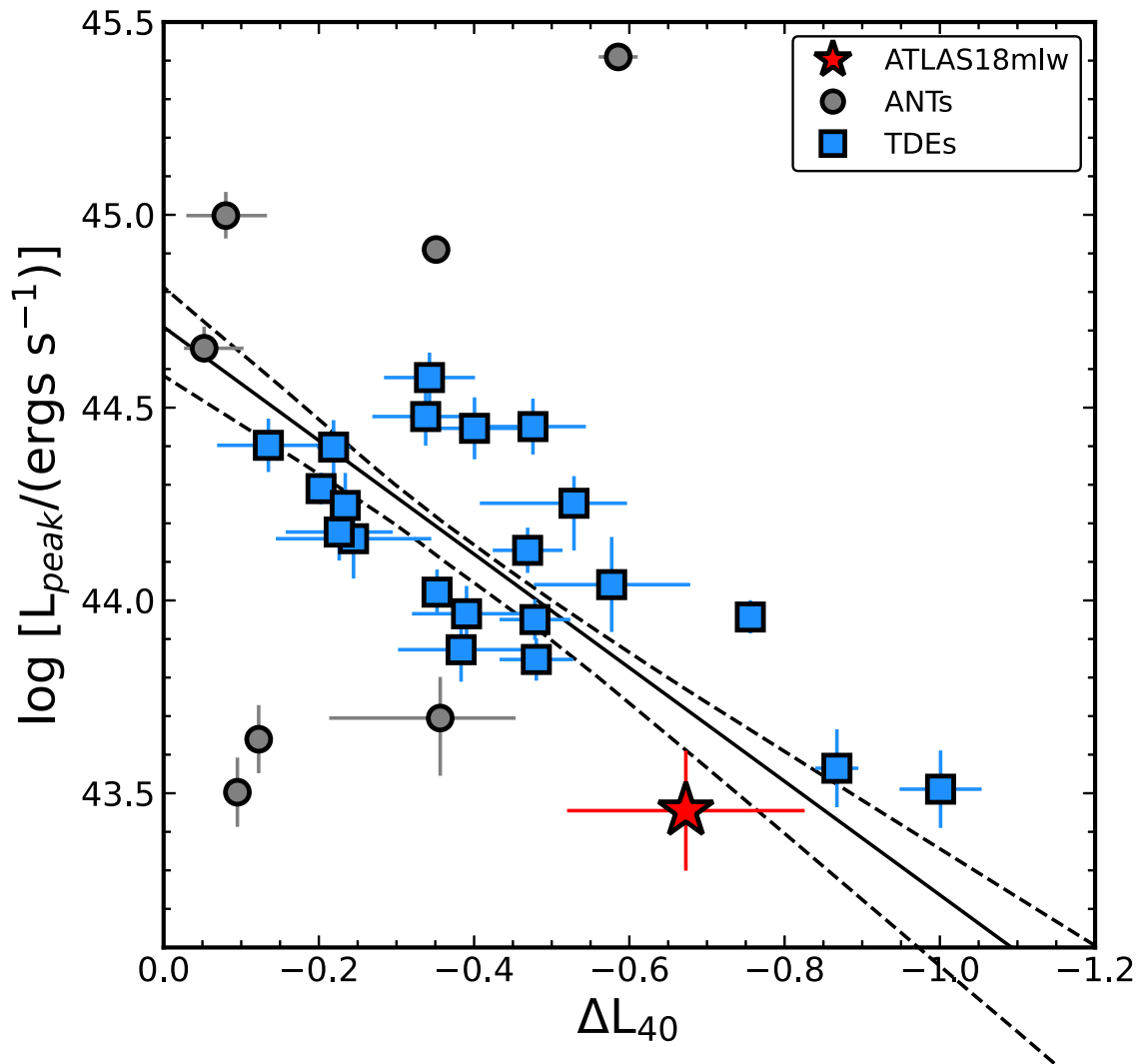
Figure 6. Peak bolometric luminosity versus the decline rate of several TDEs (blue squares) and ANTs (grey circles). The decline rate ΔL_{40} is the difference between the log of the peak luminosity and the log of the luminosity at 40 d after peak (Hinkle et al. 2020). ATLAS18mlw is shown with a red star, and the uncertainties here are 90 per cent confidence intervals.

detected. Many TDEs show an increase in line luminosity near or shortly after peak light before declining (Charalampopoulos et al. 2022a), although here we only have a single spectrum with which to constrain the line emission.

The temperature derived from our blackbody fit, $\log(T[K]) = 4.06 \pm 0.01$, is towards the low end of temperatures for the TDE-H subclass (van Velzen et al. 2021; Hammerstein et al. 2022). However, the lack of UV photometry makes the systematic errors on our temperature significantly higher than the statistical errors from the blackbody fit alone. None the less, both the TDE-He and TDE-Bowen classes have much higher median temperatures, by ∼35 per cent and ∼40 per cent, respectively, thus supporting this object belonging to the TDE-H class. Additionally, the estimated blackbody radius of $\log(R [cm]) = 15.07 \pm 0.02$ is fully consistent with the radii of the TDE-H objects. van Velzen et al. (2021) find that the separation between TDE-H and TDE-Bowen is strongest for the blackbody radius, again supporting a TDE-H nature. Still, if our crude blackbody fit without UV photometry underestimates the temperature, then the blackbody radius may be overestimated for a similar luminosity.

In terms of the bolometric evolution, we find that ATLAS18mlw is most similar to the 'faint and fast' TDEs iPTF16fnl (Blagorodnova et al. 2017; Brown et al. 2018), ZTF19abzrhgq (AT2019qiz; Nicholl et al. 2020), AT2020neh (Angus et al. 2022), and AT2020wey (Charalampopoulos et al. 2022b). Of these TDEs, ATLAS18mlw has the second lowest peak luminosity, although the bolometric luminosity estimate is the weakest as there is no UV data to confirm the temperature. ATLAS18mlw is also the only likely TDE-H object of these faint and fast TDEs. The decline rate of ATLAS18mlw indicates that it is a fast-evolving TDE, with only a small number of sources declining faster. These are iPTF16fnl, ZTF19abzrhgq, ASASSN-14ae (Holoien et al. 2014), and AT2020wey. Several studies have suggested that faint and fast TDEs may be tied to lower mass SMBHs (Blagorodnova et al. 2017), potentially as a result of more efficient outflow launching around such SMBHs (Nicholl et al. 2020). The SMBH mass for ATLAS18mlw is similar to, but slightly lower than other TDEs (Wevers et al. 2017; Nicholl et al. 2022), although the estimate is only based on the total stellar mass from SPS fitting, and therefore has a large uncertainty.

It is also interesting to note that the position of ATLAS18mlw in peak-luminosity/decline-rate space is much more similar to the TDEs than any of the ANTs shown on Fig. 6. Recently, Charalampopoulos et al. (2022b) measured the decline rate of another faint and fast TDE AT2020wey and find it to be $\Delta L_{40} = -1.28$, fully consistent with this relationship. These results support using the $\log(L_{peak}) - \Delta L_{40}$ parameter space to help us differentiate between different classes of transients even without abundant data during the event, as will be the case for many discoveries by the Legacy Survey of Space and Time (LSST; Ivezić et al. 2019) on the Vera Rubin Observatory.

For the case of ATLAS18mlw, the late identification as a TDE precluded any follow-up observations, highlighting the need for rapid response to newly discovered nuclear transients. As the discovery of TDEs continues to expand, it is important to prioritize data that best help us understand physics driving the observed emission. Optical spectroscopy and high-energy UV/X-ray photometry (e.g. Mushotzky 2018; Kulkarni et al. 2021), ideally beginning prior to peak light, are necessary to understand the detailed properties of individual events.

This goal requires the expansion of spectroscopic classification surveys to match the growing flood of transient discoveries each night. Even now, the number of discovered transients is roughly an order-of-magnitude higher than the number of transients classified spectroscopically. One obvious improvement is the robotizing of existing classification surveys to improve efficiency. For instance, the SCAT survey (Tucker et al. 2022) is currently classically scheduled and observed with 323 classifications in the last year, representing ~13 per cent of all classified transients. After the ongoing robotizing of the UH88 telescope[5] is completed in late 2022, this number is expected to increase to ~1200 per yr.

Sources like ATLAS18mlw show that even with minimal data, important conclusions can be drawn and comparisons to very well-studied objects can be made. In particular, the host galaxies of sources like ATLAS18mlw can and should be incorporated into TDE population studies as these samples grow, although quantification of the reliability of source classifications as TDEs will be important.

ACKNOWLEDGEMENTS

DATA AVAILABILITY

The data underlying this article will be shared on reasonable request to the corresponding author.

Facilities: ASAS-SN (Shappee et al. 2014; Kochanek et al. 2017), ATLAS (Tonry et al. 2018), GMOS (Hook et al. 2004), SNIFS (Lantz et al. 2004), ZTF (Bellm et al. 2019).

Software: LINMIX (Kelly 2007), MATPLOTLIB (Hunter 2007), NUMPY (Harris et al. 2020), PYPHOT, PPXF (Cappellari & Emsellem 2004; Cappellari 2017), SCIPY (Virtanen et al. 2020).

REFERENCES

Aguado D. S. et al., 2019, ApJS, 240, 23
Alard C., 2000, A&AS, 144, 363
Alard C., Lupton R. H., 1998, ApJ, 503, 325
Aldering G. et al., 2006, ApJ, 650, 510
Angus C. R. et al., 2022, Nat. Astron., 6, 1452
Antonucci R., 1993, ARA&A, 31, 473
Arcavi I. et al., 2014, ApJ, 793, 38
Arcavi I., Nyiha I., French K. D., 2022, ApJ, 924, 121
Assef R. J. et al., 2013, ApJ, 772, 26
Auchettl K., Guillochon J., Ramirez-Ruiz E., 2017, ApJ, 838, 149
Auchettl K., Ramirez-Ruiz E., Guillochon J., 2018, ApJ, 852, 37
Baldwin J. A., Phillips M. M., Terlevich R., 1981, PASP, 93, 5
Barbarino C., Carracedo A. S., Tartaglia L., Yaron O., 2019, Transient Name Server Classification Report, 2019-287, 1
Barron J. T., Stumm C., Hogg D. W., Lang D., Roweis S., 2008, AJ, 135, 414
Bellm E. C. et al., 2019, PASP, 131, 018002
Bennett C. L., Larson D., Weiland J. L., Hinshaw G., 2014, ApJ, 794, 135
Blagorodnova N. et al., 2017, ApJ, 844, 46
Bongiorno A. et al., 2010, A&A, 510, A56
Brown J. S. et al., 2018, MNRAS, 473, 1130
Brown J. S., Holoien T. W.-S., Auchettl K., Stanek K. Z., Kochanek C. S., Shappee B. J., Prieto J. L., Grupe D., 2017, MNRAS, 466, 4904
Bruzual G., Charlot S., 2003, MNRAS, 344, 1000
Cappellari M., 2017, MNRAS, 466, 798
Cappellari M., Emsellem E., 2004, PASP, 116, 138
Cardelli J. A., Clayton G. C., Mathis J. S., 1989, ApJ, 345, 245
Chambers K. C. et al., 2016, preprint (arXiv:1612.05560)
Charalampopoulos P. et al., 2022a, A&A, 659, A34
Charalampopoulos P., Pursiainen M., Leloudas G., Arcavi I., Newsome M., Schulze S., Burke J., Nicholl M., 2022b, preprint (arXiv:2209.12913)
Cid Fernandes R., Stasińska G., Mateus A., Vale Asari N., 2011, MNRAS, 413, 1687
Eisenstein D. J. et al., 2011, AJ, 142, 72
Evans C. R., Kochanek C. S., 1989, ApJ, 346, L13
Filippenko A. V., 1997, ARA&A, 35, 309
Folatelli G. et al., 2010, AJ, 139, 120

Frederick S. et al., 2021, ApJ, 920, 56
Fremling C. et al., 2020, ApJ, 895, 32
Fremling C. et al., 2021, ApJ, 917, L2
French K. D., 2021, PASP, 133, 072001
French K. D., Arcavi I., Zabludoff A. I., Stone N., Hiramatsu D., van Velzen S., McCully C., Jiang N., 2020a, ApJ, 891, 93
French K. D., Arcavi I., Zabludoff A., 2016, ApJ, 818, L21
French K. D., Wevers T., Law-Smith J., Graur O., Zabludoff A. I., 2020b, Space Sci. Rev., 216, 32
French K. D., Yang Y., Zabludoff A. I., Tremonti C. A., 2018, ApJ, 862, 2
Gafton E., Rosswog S., 2019, MNRAS, 487, 4790
Galbany L. et al., 2016, AJ, 151, 33
Gezari S. et al., 2017, ApJ, 835, 144
Gezari S., 2021, ARA&A, 59, 21
Graham A. W., Erwin P., Caon N., Trujillo I., 2001, ApJ, 563, L11
Graur O., French K. D., Zahid H. J., Guillochon J., Mandel K. S., Auchettl K., Zabludoff A. I., 2018, ApJ, 853, 39
Grishin E., Bobrick A., Hirai R., Mandel I., Perets H. B., 2021, MNRAS, 507, 156
Hammerstein E. et al., 2022, preprint (arXiv:2203.01461)
Harris C. R. et al., 2020, Nature, 585, 357
Hayden B. et al., 2021, ApJ, 912, 87
Heckman T. M., 1980, A&A, 500, 187
HI4PI Collaboration, 2016, A&A, 594, A116
Hinkle J. T. et al., 2021b, MNRAS, 500, 1673
Hinkle J. T., Holoien T. W. S., Shappee B. J., Auchettl K., 2021a, ApJ, 910, 83
Hinkle J. T., Holoien T. W. S., Shappee B. J., Auchettl K., Kochanek C. S., Stanek K. Z., Payne A. V., Thompson T. A., 2020, ApJ, 894, L10
Ho L. C., 2008, ARA&A, 46, 475
Holoien T. W. S. et al., 2020, ApJ, 898, 161
Holoien T. W.-S. et al., 2014, MNRAS, 445, 3263
Holoien T. W.-S. et al., 2016, MNRAS, 455, 2918
Holoien T. W.-S., Brown J. S., Auchettl K., Kochanek C. S., Prieto J. L., Shappee B. J., Van Saders J., 2018, MNRAS, 480, 5689
Hook I. M., Jørgensen I., Allington-Smith J. R., Davies R. L., Metcalfe N., Murowinski R. G., Crampton D., 2004, PASP, 116, 425
Hunter J. D., 2007, Comput. Sci. Eng., 9, 90
Ivezić Ž. et al., 2019, ApJ, 873, 111
Kauffmann G. et al., 2003, MNRAS, 346, 1055
Kelly B. C., 2007, ApJ, 665, 1489
Kelson D. D., Illingworth G. D., van Dokkum P. G., Franx M., 2000, ApJ, 531, 159
Kewley L. J., Dopita M. A., Sutherland R. S., Heisler C. A., Trevena J., 2001, ApJ, 556, 121
Kewley L. J., Groves B., Kauffmann G., Heckman T., 2006, MNRAS, 372, 961
Kochanek C. S. et al., 2017, PASP, 129, 104502
Kriek M., van Dokkum P. G., Labbé I., Franx M., Illingworth G. D., Marchesini D., Quadri R. F., 2009, ApJ, 700, 221
Kulkarni S. R. et al., 2021, preprint (arXiv:2111.15608)
Lacerda E. A. D., Sánchez S. F., Cid Fernandes R., López-Cobá C., Espinosa-Ponce C., Galbany L., 2020, MNRAS, 492, 3073
Lang D., Hogg D. W., Mierle K., Blanton M., Roweis S., 2010, AJ, 139, 1782
Lantz B. et al., 2004, in Mazuray L., Rogers P. J., Wartmann R., eds, Proc. SPIE Conf. Ser. Vol. 5249, Optical Design and Engineering. SPIE, Bellingham, p. 146
Law-Smith J., Ramirez-Ruiz E., Ellison S. L., Foley R. J., 2017, ApJ, 850, 22
Leloudas G. et al., 2019, ApJ, 887, 218
Lusso E. et al., 2012, MNRAS, 425, 623
Martin D. C. et al., 2005, ApJ, 619, L1
McConnell N. J., Ma C.-P., 2013, ApJ, 764, 184
Mendel J. T., Simard L., Palmer M., Ellison S. L., Patton D. R., 2014, ApJS, 210, 3
Million C. et al., 2016, ApJ, 833, 292
Mockler B., Guillochon J., Ramirez-Ruiz E., 2019, ApJ, 872, 151

Mockler B., Twum A. A., Auchettl K., Dodd S., French K. D., Law-Smith J. A. P., Ramirez-Ruiz E., 2022, ApJ, 924, 70
Mushotzky R., 2018, in den Herder J.-W. A., Nikzad S., Nakazawa K., eds, Proc. SPIE Conf. Ser. Vol. 10699, Space Telescopes and Instrumentation 2018: Ultraviolet to Gamma Ray. SPIE, Bellingham, p. 1069929
Neustadt J. M. M. et al., 2020, MNRAS, 494, 2538
Nicholl M. et al., 2020, MNRAS, 499, 482
Nicholl M., Lanning D., Ramsden P., Mockler B., Lawrence A., Short P., Ridley E. J., 2022, MNRAS, 515, 5604
Osterbrock D. E., 1989, Astrophysics of Gaseous Nebulae and Active Galactic Nuclei. University Science Books, Sausalito, CA
Osterbrock D. E., Ferland G. J., 2006, Astrophysics of Gaseous Nebulae and Active Galactic Nuclei. University Science Books, Sausalito, CA
Pennell A., Runnoe J. C., Brotherton M. S., 2017, MNRAS, 468, 1433
Phinney E. S., 1989, Nature, 340, 595
Poznanski D., Prochaska J. X., Bloom J. S., 2012, MNRAS, 426, 1465
Prieto J. L. et al., 2016, ApJ, 830, L32
Rees M. J., 1988, Nature, 333, 523
Reines A. E., Volonteri M., 2015, ApJ, 813, 82
Ricci C. et al., 2017, ApJS, 233, 17
Ricker G. R. et al., 2015, J. Astron. Telesc. Instrum. Syst., 1, 014003
Roth N., Kasen D., 2018, ApJ, 855, 54
Ryu T., Krolik J., Piran T., 2020, ApJ, 904, 73
Salpeter E. E., 1955, ApJ, 121, 161
Schlafly E. F., Finkbeiner D. P., 2011, ApJ, 737, 103
Shappee B. J. et al., 2014, ApJ, 788, 48
Smartt S. J. et al., 2015, A&A, 579, A40
Smith K. W. et al., 2020, PASP, 132, 085002
Stone N. C., Metzger B. D., 2016, MNRAS, 455, 859
Stone N. C., van Velzen S., 2016, ApJ, 825, L14
Tonry J. L. et al., 2018, PASP, 130, 064505
Tonry J., 2018, Transient Name Server Discovery Report, 2018-356, 1
Tucker M. A. et al., 2022, preprint (arXiv:2210.09322)
Tucker M. A., Huber M., Shappee B. J., Dong S., Bose S., Chen P., 2018, Astron. Telegram, 11444, 1
Ulmer A., 1999, ApJ, 514, 180
Vallely P. J. et al., 2019, MNRAS, 487, 2372
Vallely P. J., Kochanek C. S., Stanek K. Z., Fausnaugh M., Shappee B. J., 2021, MNRAS, 500, 5639
van Velzen S. et al., 2021, ApJ, 908, 4
van Velzen S., 2018, ApJ, 852, 72
van Velzen S., Farrar G. R., 2014, ApJ, 792, 53
van Velzen S., Holoien T. W. S., Onori F., Hung T., Arcavi I., 2020, Space Sci. Rev., 216, 124
van Velzen S., Stone N. C., Metzger B. D., Gezari S., Brown T. M., Fruchter A. S., 2019, ApJ, 878, 82
Vanden Berk D. E. et al., 2001, AJ, 122, 549
Vanderspek R. et al., 2018, TESS Instrument Handbook, Tech. rep.. Kavli Institute for Astrophysics and Space Science, Massachusetts Institute of Technology, Cambridge, MA
Veilleux S., Osterbrock D. E., 1987, ApJS, 63, 295
Virtanen P. et al., 2020, Nat. Methods, 17, 261
Voges W. et al., 1999, A&A, 349, 389
Wang J., Merritt D., 2004, ApJ, 600, 149
Wevers T., van Velzen S., Jonker P. G., Stone N. C., Hung T., Onori F., Gezari S., Blagorodnova N., 2017, MNRAS, 471, 1694
Woo J.-H., Urry C. M., 2002, ApJ, 579, 530
Wright E. L. et al., 2010, AJ, 140, 1868
Wright E. L., 2006, PASP, 118, 1711
Wyrzykowski Ł., Hodgkin S., Blogorodnova N., Koposov S., Burgon R., 2012, in 2nd Gaia Follow-up Network for Solar System Objects, p. 21
Zakamska N. L. et al., 2003, AJ, 126, 2125

This paper has been typeset from a TEX/LATEX file prepared by the author.